Bulgarian Journal of Physics vol. **XX** (20XX) 1–26

Surface-Enhanced Raman Spectroscopy of Neonicotinoid Insecticides

P.A. Atanasov[1], **N.N. Nedyalkov**[1*], **N. Fukata**[2], **W. Jevasuwan**[2]
[1]Institute of Electronics, Bulgarian Academy of Sciences, Sofia, Bulgaria
[2]International Center for Materials for Nanoarchitectonics (MANA),
National Institute for Materials Science (NIMS), Tsukuba, Japan
[*]Corresponding author Email: nnn_1900@yahoo.com

Received *25 March 2025*

Abstract. This review summarizes our progress and effort in the study during last seven years of one of the very important class of insecticides – neonicotinoids, which are considered as the most effective ones. Advanced active substrates of Au and Ag nanoparticles were produced by pulsed-laser deposition and thermal deposition on different basic substrates as Si wafers, quartz, paper, aluminum ceramic or diamond abrasive films in view of surface-enhanced Raman spectroscopy (SERS) detection of the studied neonicotinoids. The SERS peaks intensity rose by at least one order of magnitude after the pulsed-laser annealing of the nobble metal films or nanoparticles ar-rays formation. In all cases, the neonicotinoid insecticides in amounts much smaller than those ordinarily applied in agricultural medicine were studied. The enhancement factor (EF) was estimated to be about $\approx 10^5$ (thiamethoxam) as the limit of detection (LOD) reached tenths of ≈nM (thiamethoxam and imidacloprid). The importance of SERS as a relatively inexpensive and simple method is emphasized in monitoring, controlling and regulating the level of such substances as environmental pollutants, thus precluding harming the honey bees' health and thus the human health.

KEY WORDS: neonicotinoid insecticides, silver and gold nano-structures, surface-enhanced Raman spectroscopy, pulsed laser or thermal deposition.

1 Introduction

The neonicotinoids (neonics) are chemically similar to the nicotine and are considered the most effective class of active substances used in the agriculture for plant protection against harmful insects. They were developed by "Shell" and "Bayer" in the 1980s [1]. The neonics were accepted for use in EU since 2005. Additionally, one of them, namely, imidacloprid has been the most extensively used insecticide since 1999 until at least 2018. The modern agriculture is unthinkable without application of different type of insecticides. According to Environmental Protection Agency (EPA) the annual production and market of insecticides exceeds 50 billion US dollars.

Neonics, as well nicotine, bind to nicotinic acetylcholine cell receptors and causes its response [2, 3]. In mammals, the nicotinic acetylcholine receptors are situated in the cells of the central and peripheral nervous systems. In contrast, in insects (including bees), these receptors are located in the central nervous system only. These receptors are turned on by a neurotransmitter, namely, acetylcholine, and although their low-to-moderate activation induces nervous stimulation, i.e. high-level overestimation and blocking them. Finally, these result in paralysis and death. The enzyme acetyl cholinesterase prevents acetylcholine from terminating signals from these receptors. Moreover, the acetyl cholinesterase is not capable of breaking down neonics, so that their binding becomes irreversible. Neonics residues gather in the treated plants' pollen and nectar and thus creating potential risks to pollinators. In what concerns honeybees, not only are they of outstanding significance to the ecology, but they have economic impact as well, providing ingredients for medicinal purposes. In spite of their doubtless importance, honeybees are at risk of becoming an endangered species because of biotic and abiotic stressors. The honeybees' conservation is a challenge necessitating worldwide cooperation. Thus, the EU and USA undertook extensive research and measures to prevent the reduction and disappearance of the bees' colonies [4–6]. As result of wide studies and discussions, the neonics thiamethoxam, imidacloprid and clothianidin, were banned by the European Food Safety Authority for outdoor use since May 2018 [6].

Variety of methods and systems for monitoring neonics were described by several authors. Some of them are following. A systematic review of the analytical methods for studies of risk management and risk assessment of neonicotinoid insecticides was reported by Watanabe [7]. Here, analytical methods based on chromatographic and nonchromatographic techniques were described and summarized. The infrared and Raman spectra of imidacloprid were predicted via quantum level simulations and compared them with experimental results. [8, 9] Several experimental approaches were reviewed by Ahmed et al. [10].

Using complicated methods based on the automated flow fluorescent immunoassay, a sensitivity of 30 pg/ml thiamethoxam was reported by Kim et al. [11], and enzyme immunoassay using enzyme-labelled antigens a sensitivity of 0.5 ng/ml thiamethoxam was achieved [12], respectively. Later on, a very advanced and detailed experimental study of thiamethoxam, that is, FT-IR, FT-Raman, and UV-VIS study based on the density functional theory, and ab initio Restricted Hartree–Fock has been performed and reported by Zhang et al. [13]. An optimized geometrical structure of the molecule spectroscopy, as well as theoretical and harmonic frequencies was calculated, and the complete assignments of the observed spectra were proposed as well.

Surface-enhanced Raman diagnostic membranes were used for SERS study of several insecticides, among which is the thiacloprid [14]. Phifer analyzed apple samples for insecticide residues and applied the generated calibration curves to quantify the presence of the residues [15]. Minimum concentration of 12.4

parts per billion (ppb) (12.4 mg/L) was detected, which is below the insecticide residue tolerance levels for apples stated by the U.S. Environmental Protection Agency. In addition, several aptamers were also used to functionalize Au sensor chips in order to improve sensitivity. An advanced and detailed experimental study of thiacloprid was reported by Cañamares and Feis [16], which included Raman and SERS spectroscopy of this chemical in solid form, in acetone solution, and adsorbed onto Ag and Au hydrosols concentrations as low as mM. Moreover, they applied density functional theory to calculate how the individual stable molecular structure reflects on the Raman spectra and interpreted the difference between SERS and Raman spectra as well as the possible interactions between this molecule and the metal surface which form iminocyano group. Finally, comparison between experimental and theoretical results was provided. Furthermore, Chamuah et al. [17] reported on the preparation of advanced active SERS substrates of Au-coated electrospun polyvinyl alcohol nanofibers for study of mainly malachite green, but thiacloprid as well. The minimum concentration detectable achieved was 0.2658 ppm (265.8 mg/L). Finally, Ag-coated Au NPs were used for SERS detection of thiacloprid residue or mixture with other pesticides in standard solution and on peach [18].

Imidacloprid is probably the most studied neonic. Different methods have widely been used in order to study imidacloprid in plants and agricultural products using liquid chromatography coupled to mass spectrometry [19]. Quintás et al. [20] have applied Fourier transform infrared technique in order to determine the imidacloprid in pesticide formulations and the results were statistically compared to those found by high performance liquid chromatography. The limit of detection achieved was about 9 lg/g. Several imaging techniques have also been suggested and used for imidacloprid detection on botanic surfaces. For example, Gerbig et al. [21] have tested desorption electrospray ionization mass spectrometry for detection of insecticide on leaves and stem segments. Using this method only qualitative results were achieved. Moreover, near-infrared spectroscopy was used for imaging of imidacloprid in artificial powders and commercial formulation [22]. This method allowed successful quantification from 5% to 99.99% imidacloprid in powders. Lee et al. [23] combined an indirect competitive immunoassay, highly sensitive surface plasmon resonance biochip and a simple portable imaging setup for label-free detection of imidacloprid. The authors proposed that precise semi-quantitative analyses at very low detection limit can further be completed by using image processing in a smartphone.

Multiphoton electron extraction spectroscopy was successfully applied for imaging and quantification of imidacloprid on plants and other surfaces [24]. This method was proven to be fast and provided low detection limits (down to nanogram level) and can be directly performed with no sample pretreatment. With this, it is a good candidate for field analyses. In the advanced papers of Moreira et al. [8, 9] the development and application of quantum level simulations were described in order to predict infra-red and Raman spectra of the most stable con-

former of imidacloprid. Four molecular geometries have been investigated via density functional theory approach employing the hybrid meta functional M06-2X and hybrid functional B3LYP. The M062X/PCM model was proved to be the best to predict structural features, while the values of harmonic vibrational frequencies were predicted more accurately using the B3LYP functional. The theoretical results were compared with the Infrared and Raman spectroscopy measurements. Several experimental investigations of imidacloprid residues have been carried out applying surface-enhance Raman spectroscopy (SERS) analyses at different configurations [25, 27, 36]. Zhang et al. [25] fabricated gold nanoparticle functionalized glycidyl methacrylate-ethylene dimethacrylate suspension as SERS arrays and measured several pesticides, among which imidacloprid, at concentration of 10 mg/L. Dowgiallo et Guenther [26] have obtained SERS spectra of residue of several insecticides on fruit surfaces and Hou et al. [27] have applied SERS for imidacloprid monitoring as the limit of detection of 0.5 lg/cm^2 was achieved for tea leaves and 0.02 lg/cm^2 for apple peel, respectively. Some other studies were also published [28, 29]. Tang et al. [28] have used silver nanoparticles coated glass bead as nonplanar substrate for SERS sensing. An imidacloprid concentration of 0.05 mg/L was detected. Highly roughed surface of flower-shaped silver nanostructure was developed as SERS active substrates and applied by Chen et al. [29] for testing imidacloprid residue in tea. A minimum concentration down to 1.0×10^{-4} lg/mL was detected.

In the recent decades, the surface-enhanced Raman spectroscopy (SERS) has be-come a potent tool for a high-sensitivity detection of small quantities of a wide variety of materials. It relies on the enormous Raman signal enhancement arising from molecules that are in a close proximity of (adsorbed by) metal nanostructures. Thus, the electromagnetic field interacts with the metal nanostructures (NSs) and causes a collective coherent oscillation of the free electrons, i.e., a plasmon resonance takes place. This resonance for Ag and Au is in the UV and visible spectral ranges giving rise to sharp absorption and scattering spectra [30–32].

Silver and gold nanoparticle (NP) arrays still attract widespread attention due to their unique properties and functionalities compared with their corresponding bulk materials. The electromagnetic field (EM) in the close vicinity of the metal nanostructures expresses specific properties, when electromagnetic wave irradiates the system. The intensity of the EM field could be few orders of magnitude stronger compared with the incident one and decreases rapidly with the distance from nanostructure, so it is localized in the vicinity around the metal surface [33, 34]. Therefore, the spatial characteristics of this field are defined by the structure size, but not by the incident wavelength [35]. The properties of such 2D structures strongly depend on the surrounding medium, the interparticle distance, the size, and its form. The enormous enhancement of the EM field intensity around the metal nanostructures area has been used in one of the most important applications – surface enhanced Raman spectroscopy (SERS) [36,37].

This technique has been used for detection and analysis of broad range of explosives, drugs, water and food pollutions, viruses and bacteria, DNA, and single molecule [38, 39]. It is worth noting that more than a decade the Van Duyne group has been making great effort on different aspects of SERS investigations and different applications [39–42].

The plasmon resonance energy is strongly affected by the NSs composition and morphology. It is well known that one of the important ways to increase the sensitivity is the choice of the proper substrate on which the noble metal NPs are deposited in such a way to increase the presence of SERS hotspots [43, 44].

A variety of commercial active SERS substrates are available and can be found [45–49]. Below we list just a few examples with brief characteristics: KlariteTM (Renishaw Diagnostics, UK) and Q-SERS (Nanova, USA) sensors are based on silicon wafers; SERStrate (Silmeco, DK) uses nano-structured Si as a base material covered by Ag or Au nano-pillars; P-SERS (Diagnostic anSERS, MD) is a paper-based SERS device produced by an inkjet-printed technology; J12 853 (Hamamatsu Photonics, JP) is a SERS sensor based on nano-structured Au formed by nano-imprinting technology; the Horiba Scientific SERS substrates are coated with Au nanorods by oblique dynamic vacuum evaporation; the Ocean Optics SERS substrates (Ocean Optics, Fl) are based on an Au or Ag active element on glass. Unfortunately, all commercial SERS substrates are still relatively expensive.

The purpose of the following review is to summarize our results on preparation of advanced Ag and Au films and nanostructures by laser or thermal deposition methods on basic substrates as Si wafers, quartz, paper, aluminum ceramic or diamond abrasive films [50]. The as produced advanced substrates were used for high-resolution SERS analysis of the neonicotinoid insecticide as thiamethoxam [51–53], thiacloprid [54], acetamiprid [55], and imidacloprid [50, 56]. Several diminishing concentrations of the analytes below the level of the use in the agriculture were detected and the performance of all types of different substrates were compared. The enhancement factor (EF) was estimated to be about $\approx 10^5$ (thiamethoxam) and the limit of detection (LOD) reached tenths of $\approx$ nM (thiamethoxam and imidacloprid).

2 Materials and Methods

2.1 Synthesis of advanced Ag and Au active substrates

The Ag and Au films or nanostructures (NSs) were sanitized by thermal or pulsed-laser depositions on the following initial substrates: two types Si wafers (polished by means of 1-μm grade powder, and its back side left as purchased); (001)SiO_2; printer paper; aluminum ceramic; manually dry scratched in advance of quartz substrates using three grades (0.1, 0.5, or 1 μm) of diamond supper-

abrasive slurry coated on high precision polyester diamond abrasive films; high precision diamond abrasive films. The Ag and Au films of different thicknesses were grown in vacuum (pressure of ~10^{-3} Pa) at room temperature by standard pulsed-laser deposition using a Q-switched Nd:YAG laser (third harmonic, λ = 355 nm), pulse duration 12 ns and usual energy density of 3 J cm^{-2}. The thermal deposition was conducted under the same ambient conditions, with the Ag and Au films thickness being different depending the duration of the heating. Prior to deposition, the wafers were cleared by alcohol, washed by de-ionized water and dried. In some cases, the films were annealed after deposition, by the same pulsed laser by up to three consecutive pulses of several hundred energy densities to form nano-structured arrays within areas of about 3 mm in diameter.

2.2 Materials and instrumentation

The following neonics at diminishing concentrations have been studied: thiamethoxam – Aktara 25 BG [51–53], thiacloprid – Calipso 480 SC [54], acetamiprid – Mospilan 20 SP [55], and imidacloprid – Nuprid 200 SP and Warrant 700 WG [56]. The chemical structures, formula and molecular mass of the investigated neonics having nitromethylene (C=$CHNO_2$), nitroguanidine (C=NNO_2) or cyanoamidine (C=NCN) moiety, as well of nicotine, are presents in Table 1.

An SU 8230 Fe SEM (Hitachi, JP) field-scanning microscope was used to explore the samples' morphology in view of estimating its effect on the SERS spectra intensity using a finite difference time domain (FDTD) simulation (OmniSim, Photon Design).

The calculation model was based on a numerical solution of the Maxwell equations at complex geometry in homogeneous systems, which consist of variety of mate-rials and environments. It has been proven to give an adequate interpretation of the near-field characteristics of the electromagnetic (EM) field in the vicinity of NSs [57–59]. The simulated system was divided into elementary cells, where the electric and magnetic field components were calculated at each time step by the scheme of Taflove et Hagness [57]. The dielectric function of the Ag and Au particles was described by the Drude model as the input parameters were taken from Johnson et Christy [60]. The excitation laser light applied has linearly polarized plane wave at wavelength of 532 nm - the same as the laser excitation of Raman spectrometer used, directed perpendicularly to the NP arrays on the active Ag and Au structures. The dielectric function of the substrate was taken from Palik [61], and the electric field intensity, which is an in-put parameter for FDTD simulation, was assumed to be 1 V/m^2. The optical properties of the Ag and Au films and NP areas were measured by optical spectrometer (Jasco V-670, Japan).

The as prepared samples were covered by a solution in water of the desired neonic at various concentrations, then dried at room temperature. Their perfor-

Table 1. Chemical structure of nicotine and some neonicotinoid insecticides studied, having nitromethylene (C=CHNO$_2$), nitroguanidine (C=NNO$_2$) and cyanoamidine (C=NCN) moiety, respectively

Neonicotinoid	**Chemical formula**	**Molecular mass (g/mol)**	**Chemical structure**	**Market name (studied)**
Nicotine	$C_{10}H_{14}N_2$	162.23	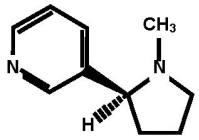	
Thiacloprid	$C_{10}H_9ClN_4S$	252.72	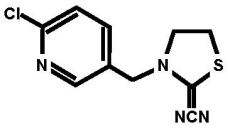	Calypso 480 SC
Imidacloprid	$C_9H_{10}ClN_5O_2$	255.661	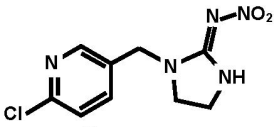	Nuprid 200 SL / Warrant 700 WG
Acetamiprid	$C_{10}H_{11}ClN_4$	222.678	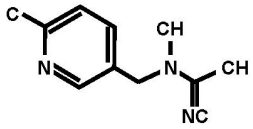	Mospilan 20SP
Thiamethoxam	$C_8H_{10}ClN_5O_3S$	291.71	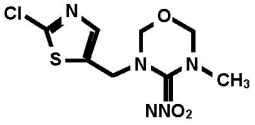	Aktara 25 BG

mance was followed by a μ-Raman spectrometer (Photon Design, Japan) at 0.5 mW usual excitation power and wavelength of 532 nm. The resolution achieved was 0.2 cm^{-1}, with the exciting laser-beam spot size on the samples surface beings ~1 μm^2. In order to reduce the noise, each Raman spectrum was obtained by averaging at least between three and six scans taken from different points of the NPs arrays with a 10-min acquisition time.

3 Results and Discussions

3.1 Morphological properties of the Ag and Au active substrates

The morphological and optical properties (transmission spectra) strongly depend on the initial substrate. The morphologies of some Ag and Au nanostructures (NSs) arrays produced on (001) SiO_2 are depicted in Figure 1. The insets show

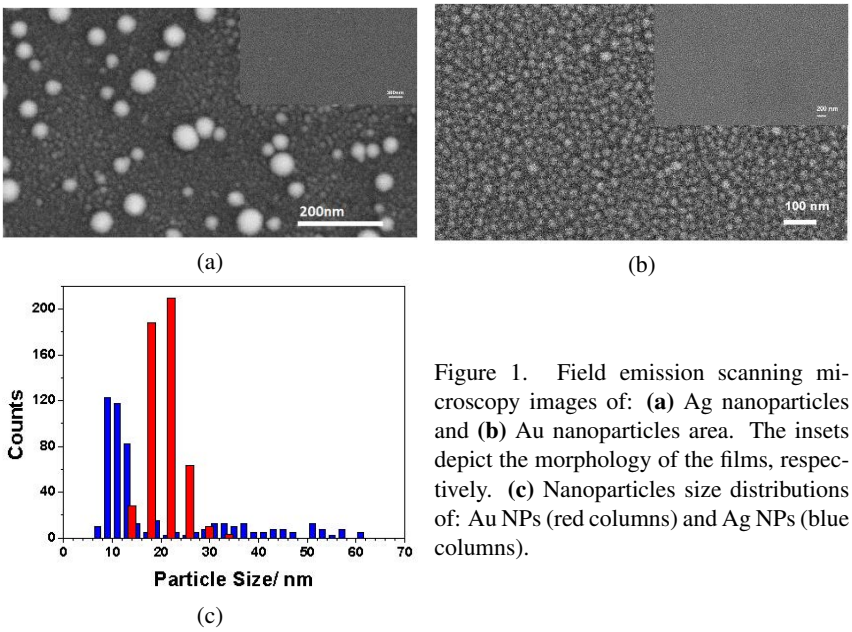

(a) (b) (c)

Figure 1. Field emission scanning microscopy images of: **(a)** Ag nanoparticles and **(b)** Au nanoparticles area. The insets depict the morphology of the films, respectively. **(c)** Nanoparticles size distributions of: Au NPs (red columns) and Ag NPs (blue columns).

the films, respectively. The size distribution (Figure 1c) evaluated by counting 500 particles has two maximums – one at ~10 nm corresponding to the smaller NPs, and second one at $30 \div 55$ nm, corresponding to the larger NPs. The Ag film is relatively flat and has fine nano-sized structure - see the inset in Figure 1a. At the contrary, the Au film has larger nano-sized structure – the inset in Figure 1b. Additionally, the Au NPs area consists of one type NPs having a maximum of the distribution at ~22 nm – Figure 1c.

The morphologies of the Ag and Au NPs areas produced on printer paper or Al_2O_3 ceramics are presented in Figure 2. In all cases the annealing leads to

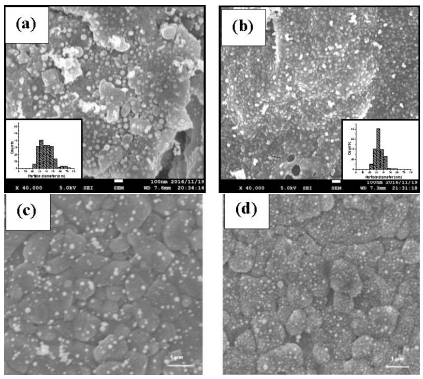

Figure 2. FE-SEM images of images of the Au NPs **(a)** and Ag NPs **(b)**, produced on printer paper. The Insets present the NPs diameter distributions, respectively. The as deposited films were irradiated by a single pulse at $\lambda = 355$ nm at fluence of 0.28 J/cm^2 [53]. SEM images **(c, d)** of Au film deposited on Al_2O_3 ceramic after annealing by one and five pulses, respectively, with fluence of 240 mJ/cm^2.

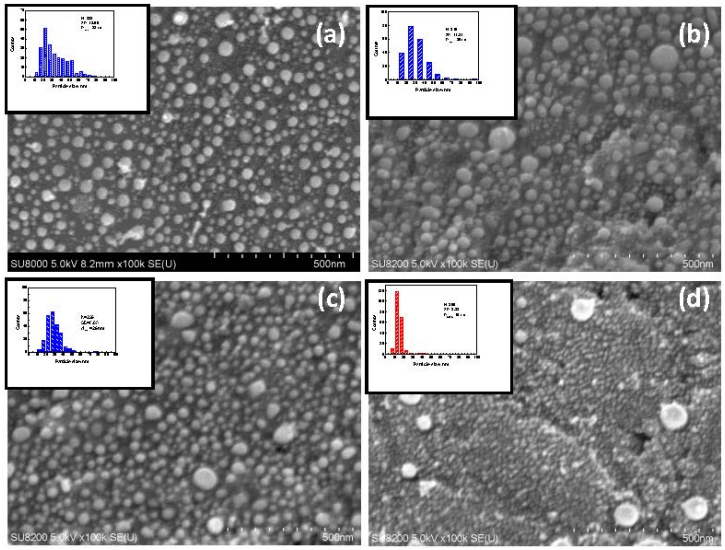

Figure 3. FE SEM images of the areas: **(a)** Thermally-deposited Ag on 1-μm polished Si and pulsed laser annealed by three pulses at 430 mJ cm^{-2}; **(b)** PLD deposited Ag (3 J cm^{-2}) on 1-μm polished Si and laser-annealed by three pulses at 400 mJ cm^{-2}; **(c)** PLD deposited (3 J cm^{-2}, 10^{-4} mbar) Ag on 1-μm polished Si and laser annealed by three pulses at 300 mJ cm^{-2}; **(d)** PLD deposited Au (3 J cm^{-2}) on 1-μm polished Si and laser-annealed by three pulses at 300 mJ cm^{-2}. The insets: **(a)**, **(b)**, **(c)** - Ag and **(d)** – Au are the nanoparticles size distributions [50].

dramatic im-prove of the quality of the surface of the films and formation of smaller nanoparticles, which finally improves the quality of the Raman spectra.

The morphologies of some other samples, after deposition Ag or Au of and pulsed-laser annealing are shown in Figure 3. As one can see, the particles distributions depend slightly on the deposition techniques, i.e., thermal (inset a) and pulsed-laser (inset b), respectively. The average dimensions values, D_{mean}, are relatively the same, namely, about ≈ 30 nm. The increasing of annealing laser-pulse energy density from 300 mJ/cm^2 to 400 mJ/cm^2 affects slightly on the NPs distribution, i.e., D_{mean} have practically the same value – see Figure 3b, c. As far as the Au area is concerned, it consists of twice as small Au particles with an average dimension $D_{\text{mean}} = 15$ nm (see inset d). In the latter case, however, there are several much larger Au nanoparticles with dimensions between 70 nm and 95 nm, whose number is less than 2% of the Au NPs measured (Figure 3d).

The results of the use back side of non-final polished Si wafer expressed similar figures. However, the NPs area of the 1 μm micro-processed Si wafer, Figure 4a, has narrower particle distribution $D_{\text{mean}} = 18$ nm, since the area of back side consists of larger NPs with $D_{\text{mean}} = 25$ nm (Figure 4b).

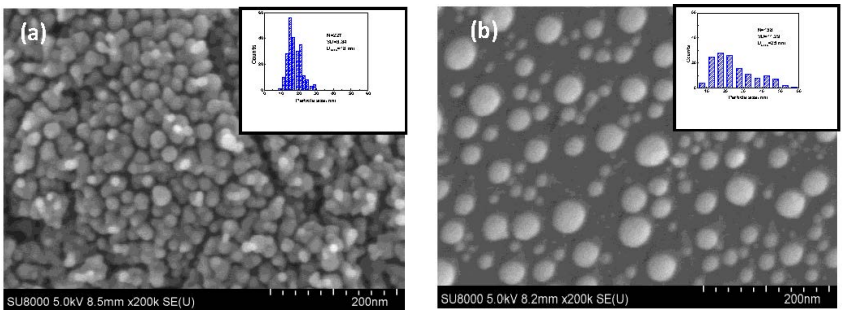

Figure 4. FE SEM pictures of thermal deposited Ag films and then pulsed laser annealed with 3 pulses at 400 mJ/cm^2 areas on the basic substrates: **(a)** 1 μm micro-processed Si and **(b)** back side of non-finish polishing Si wafer.

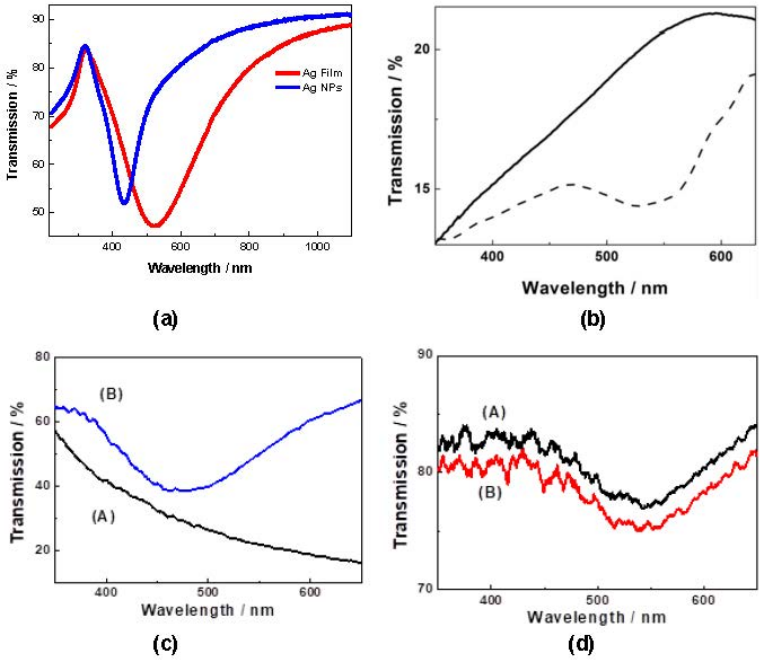

Figure 5. **(a)** Transmission spectra of Ag film and Ag NPs area produced on (001) SiO_2 [52]. **(b)** Transmission spectra of silver film, deposited on 1 mm diamond abrasive film (solid line) and laser annealed silver nanostructured area (dashed line) [56]. Transmission spectra of the films and the NSs after annealing produced on 0.5 μm grade of manually polished (100) SiO_2: **(c)** Ag film **(A)** and Ag NSs **(B)**; **(d)** Au film **(A)** and Au NSs **(B)** [55].

3.2 Optical properties of the Ag and Au active substrates

As example, some of the transmission spectra of the Ag or Au films and the NSs after annealing produced are depicted in Figure 5. The plasmon resonance is expressed especially in cases after annealing. It is usually situated around $\approx 475 \div 480$ nm for Ag films (if any) and NS and around ≈ 540 nm for Au films and Au NS, respectively. It slightly depended on the quality of the substrates.

The comparison between optical properties of the Ag and Au NPs areas can be seen from Figure 6. The plasmon resonance here is very well pronounced in both cases, i.e. the Ag and Au NPs arrays. However, it is very strong and narrow in case of Ag NPs and has lower intensity and is broader for Au NPs. The plasmon resonances are centered at 438 nm for the Ag NPs and at 568 nm for Au NPs, respectively. In case of Au film, the plasmon resonance is very shallow. However, both films have nano-structured morphology, which is a base for observation of SERS signals from the films as well. The width of the resonance band is related to the dephasing of the plasmon oscillations. The wider band width expresses lower dephasing time, which is responsible for lower near field intensity enhancement value. We assume that all the features described can induce difference in the intensity of the SERS in case of the NPs and the films.

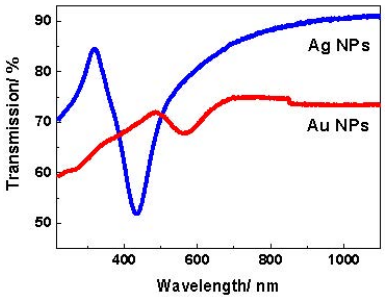

Figure 6. Transmission spectra of Ag nanoparticles (blue line) and Au nanoparticles (red line) areas.

3.3 The efficiency of the fabricated active structures on the SERS spectra – FDTD method

The efficiency of the active structures was studied and defined via FDTD simulation of the EM field intensity distribution in the vicinity of NP array using real FE SEM spectra. Here are some examples.

Different type Ag or Au NPs on SiO_2 based substrate are depicted in Figure 7 [55]. Furthermore, Ag or Au produced on three different grades of SiO_2 substrates, were depicted in Figure 8 [56]. It is seen, that in the vicinity of nanoparticles the intensity of the electrical field increases up to 10^6.

Following the results shown in Figure 8, the intensity of the peaks in SERS spectra of Ag NPs arrays were expected to have higher intensity, compared to

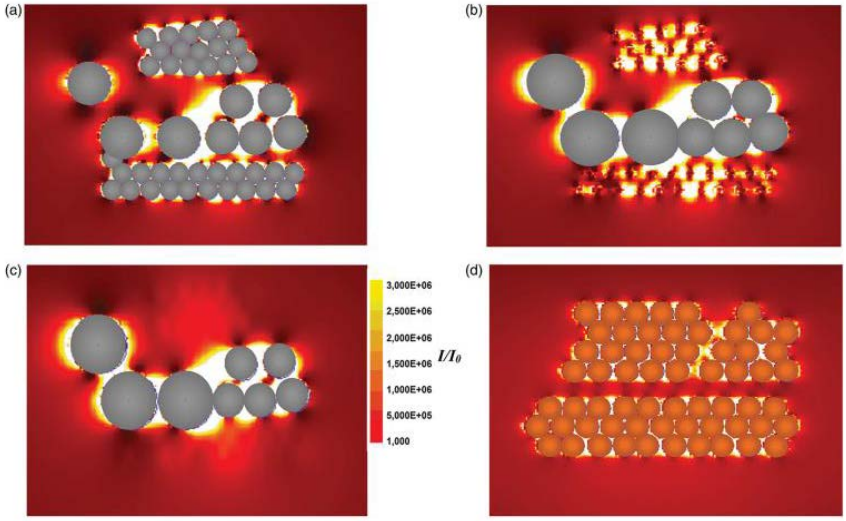

Figure 7. Calculated near field intensity distribution for imidacloprid in the vicinity of Ag **(a)**, **(b)**, and **(c)**, and Au **(d)** nanoparticle arrays by finite difference time domain simulation. The silver system consists of particles with three diameters of 10, 20, and 30 nm. In **(a)**, **(b)**, and **(c)** the distributions are given in a plane through the equator of these nanoparticles, respectively. In (d), the distribution is also given in a plane through the equator of the nanoparticles. The arrow in **(c)** indicates the polarization direction of the incident wave [55].

those of Au NPs arrays. Additionally, highest SERS intensity of Ag NPs arrays will be obtained in case of Ag covered 1 μm grade substrate and will decreases with the value of the grade of the substrate.

3.4 μ-Raman and SERS spectra of neonics

The neonics on the active Ag or Au substrate (film and NPs area) or on glass were examined by μ-Raman spectrometry. For example, Figure 9a presents comparison be-tween μ-Raman spectra of thiamethoxam (Aktara) deposited on Ag film, Ag NPs, and on glass. As is seen, several strong peaks are detected from the Ag NPs area, whereas the Ag film gives rise to some less intensive peaks. Additionally, several very week and broad peaks are observed, when analyte with a higher concentration (more than two orders of magnitude) was deposited on the glass substrate. Moreover, detailed SERS spectra of Aktara deposited on Ag NPs (Figure 9b) and on Ag film (Figure 9c) are presented. It is worth noting that no SERS signal was achieved by Au NPs.

To the best of our knowledge, a SERS study of the Aktara insecticide (thiamethoxam) is reported for the first time. The strongest peaks in the SERS spec-

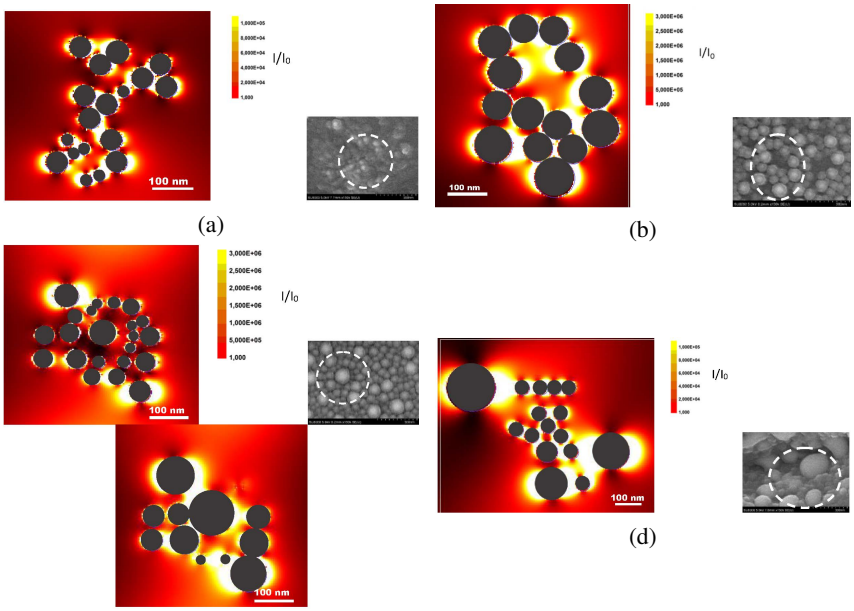

Figure 8. FDTD simulation of the EM field intensity distribution for acetamiprid in the vicinity of Ag NP array on three different grades of SiO_2 substrates: **(a)** 0.1 μm – the distribution is plane parallel to the quartz substrate at 10 nm above it; **(b)** 0.5 μm – the distribution is plane parallel to the quartz substrate at 35 nm above it; and **(c)** 1 μm - the distributions at two planes parallel to the quartz substrate at 10 nm above the surface (upper picture) and 30 nm above the surface (lower pictures). **(d)** FDTD simulation of the EM field intensity distribution in the vicinity of Au NP array on 0.5 μm grade of SiO_2 substrate – the distribution is plane parallel to the quartz substrate at 20 nm above it. The sizes and spatial distributions of the NPs were taken from the FE-SEM images adjacent [56].

tra arising from the Ag NPs sample were located between 840 and 1239 cm^{-1}. Additionally, peaks at 545, 584, and 662 cm^{-1} of intermediate intensity can be seen. According to Nicholas et al. [62], who studied other structurally related halogenated (Cl) pesticides, several peaks below 600 cm^{-1} may be ascribed to the C-Cl linkage. Moreover, the activity be-tween 600 and 1600 cm^{-1} is characteristic for hydrocarbons. The strong peak at 1620 cm^{-1} may be related to a distortion of the benzene-type ring. According to Zhang et al. [63], the strongest peaks at 901 and 1239 cm^{-1} and strong peak at 1412 cm^{-1} in the SERS coincide with the experimentally obtained peaks. Especially, the observed peak at 901 cm^{-1} may be related to the coupled C-O and C-N stretching vibrations of the benzene-type ring. Some other peaks coincide with the theoretically achieved. The vibrations in the region of 1500–1600 cm^{-1} and 1400–1625 cm^{-1} can be assigned to the ring C=N and C=C stretching mode, respectively.

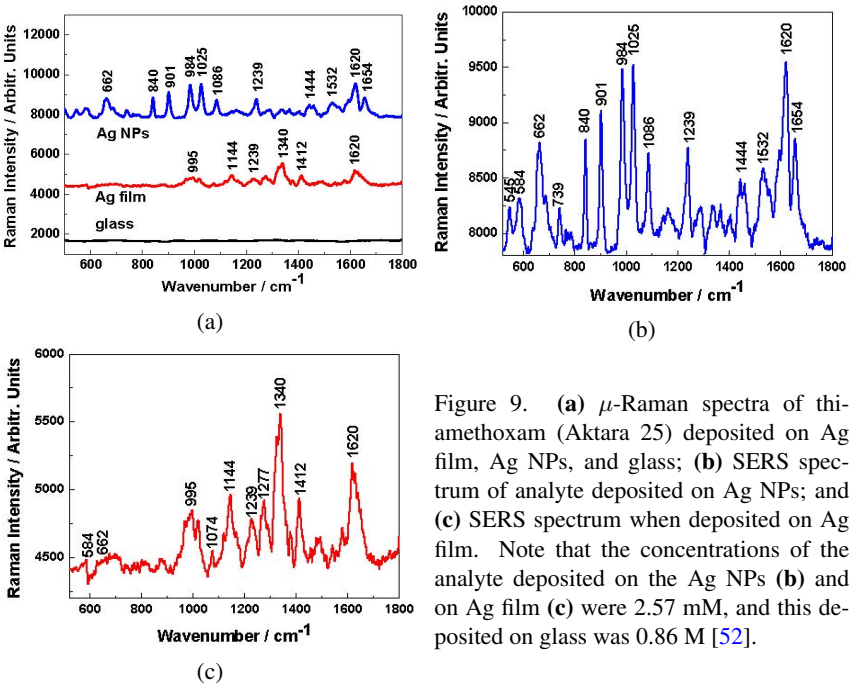

(a) (b) (c)

Figure 9. **(a)** μ-Raman spectra of thiamethoxam (Aktara 25) deposited on Ag film, Ag NPs, and glass; **(b)** SERS spectrum of analyte deposited on Ag NPs; and **(c)** SERS spectrum when deposited on Ag film. Note that the concentrations of the analyte deposited on the Ag NPs **(b)** and on Ag film **(c)** were 2.57 mM, and this deposited on glass was 0.86 M [52].

The structure of the SERS taken from NPs and films or Raman spectra from bulk materials may poses some different peaks because of morphology dependent selectivity in vibration mode excitation [64]. It is worth noting that sulphur atom in the thiamethoxam molecule may be bonded to the Ag surfaces and thus may affect the SERS spectra or shift of some peaks.

Laser annealing of Ag film on quartz substrates resulted in area containing 2-D NPs. The size distribution of the Ag NPs was much broader with two maximums at $\sim$ 10 and 30 $\div$ 55 nm. The plasmon resonance of Ag film has about the same intensity as Ag NPs, although it is much wider. To the best of our knowledge, for the first time, a strong enhancement of the μ-Raman spectra was detected in the case of Aktara 25 BG deposited on the Ag NPs area caused by plasmon resonance in Ag NPs, thus, the minimum detected concentration of thiamethoxam was evaluated to be in the order of μg/ml. The enhancement factor was estimated to be about 10^5.

Raman spectra produced of the thiacloprid on Au NPs produced by thermal deposition on Al_2O_3 ceramic initial substrates is depicted in Figure 10 [54]. It is seen that the intensity of the SERS spectra dramatically increased after laser annealing. Taking into account all SERS spectra, the deposits on the thickest Ag or Au films have higher intensities compared to those on the thinnest films. Moreover, the SERS spectra on the thinner Au films, have slightly lower inten-

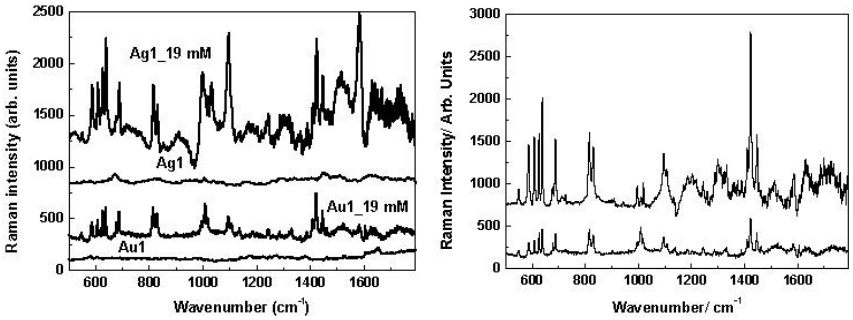

Figure 10. SERS spectra of Calypso 480 SC (thiacloprid) deposited on **(left)**: Ag or Au NSs substrates. The concentration was 19 mM in both cases. SERS spectra of clear Ag and Au NSs substrates (no analyte) are also depicted. **(right)**: Au NSs (lower spectrum) and on Au NSs (upper spectrum) after laser annealing by 5 subsequent pulses with fluence of 240 mJ/cm^2. The concentration of analyte was 19 mM in both cases [54].

sities compared to those on the thinner Ag films. Following the analyses we can to assign the vibration modes connected to the most characteristic and strongest SERS peaks.

The strong peak around 588 cm^{-1} (summarized for all samples' wavenumber shift, Δ, below 3 cm^{-1}) matches well with bending N-C≡N vibration, which also contributes to the well-expressed band around 548 cm^{-1} ($\Delta < \pm 4$ cm^{-1}) [16]. The highest wave-number shift was observed in the case of thinner Ag and Au NSs and lowest thiacloprid concentrations. Both peaks have also quite strong intensity, especially at 588 cm^{-1} in the Raman spectrum of thiacloprid deposited on glass substrates. The characteristic strong or very strong peaks around 627 cm^{-1} ($\Delta < -3$ cm^{-1}), 817 cm^{-1} ($\Delta < \pm 2$ cm^{-1}), and 1096 cm^{-1} ($\Delta < \pm 3$ cm^{-1}) can be assigned to the stretching C–Cl vibration [14]. All peaks in the SERS spectra have very small shifting with respect to those reported [14, 16]. Further-more, according to Cañamares and Feis [16] and Yaseen et al. [18], the bands observed by us around 817 and 1585 cm^{-1} can be connected with CH bending and pyridine stretching bands, respectively. Additionally, these peaks are consistent with the Raman peaks taken when the chemical was deposited on the glass substrate. The very strong bands around 1424 and 1446 cm^{-1} ($\Delta <$ 2 cm^{-1}) can be associated with the CH_2 scissoring mode [16, 18]. Both peaks can be seen in the Raman spectrum. Moreover, the peak around 688 cm^{-1} can be connected with the SERS observed peak as reported by Phifer [15] and by Cañamares and Feis [16] with a small shifting. The former indicated peak at 684 cm^{-1} as characteristic for the thiacloprid connected to the CN bending and CC deformation vibrations.

Additionally, he indicated bands at 927, 1017, and 1264 cm^{-1} are major peaks characterizing the chemical. However, the last one was not well expressed in

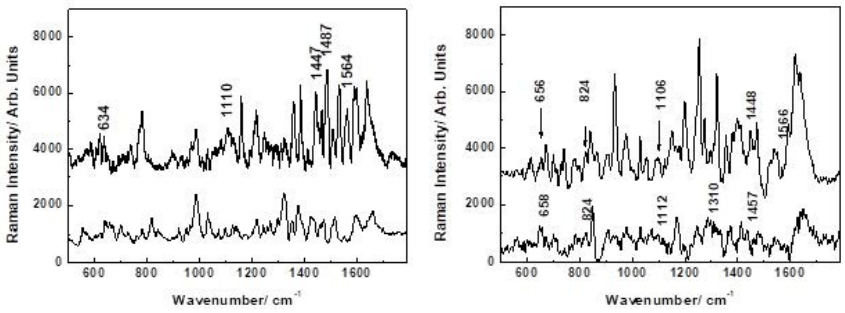

Figure 11. SERS of **(a)** Nuprid 200 SP (imidacloprid) at concentrations 7.8 mM (upper spectrum) and 390 mM (lower spectrum); **(b)** Warrant 700 WG (imidacloprid) at concentrations 5.48 mM (upper spectrum) and 274 mM (lower spectrum). The analytes were deposited on Ag NS active substrates [56].

our case and it may be these peaks with CH wagging, CH bending, and CN stretching vibrations, respectively. It is worth noting that he studied not pure thiacloprid, however, but chemical Calypso 4F via SERS diagnostic membranes, i.e. different from our substrates [15, 16]. Finally, the moderate or weak peaks around 609, 829, and 1323 cm^{-1} were indicated and can be related to those observed in the SERS spectra by Cañamares and Feis [16]. The first two peaks can be connected with the combination of different (NCN, CS, CH_2, CCN, C–Cl, and ring) vibrations. But for the last one, it can be assigned to the wagging CH_2 band. The existence of several other moderate Raman peaks at 995, 1138, 1244, and 1408 cm^{-1} in the spectra can come from the unknown inert chemicals added into insecticide Calypso 480 SC, which were not indicated by the producer.

Figure 11 depicts surface-enhance Raman spectra of imidacloprid, both studied chemicals (Nuprid 200 SP and Warrant 700 WG), deposited on alumina ceramics Ag NSs [56].

Three intensive characteristic peaks of imidacloprid for both analytes are situated at 815, 1276, and 1372 cm^{-1}. These exactly match the results of Moreira et al. [9]. Some others have very small deviation (between 2 and 4 cm^{-1}) as those of Nuprid are always shifted to the higher wavenumbers and are situated at 632, 830, 995, 1107, and 1482 cm^{-1}. These deviations can be caused by the influence of the inert unknown substances added and/or influence of the substrate. The described peaks are consistent with those published by Moreira et al. [9], Zhang et al. [25], Dowgiallo et Guenther [26], and Tang et al. [28]. However, the assignments of some vibrations proposed by the authors were different.

The comparison between the SERS spectra of acetamiprid (Mospilan 20 SP) taken from different grade (1, 0.5, and 0.1 μm) polished quartz substrates Ag NSs reveals that the highest enhancement was achieved from 1 μm grade polished SiO_2 and lowest taken from 0.1 μm, respectively. This can be deduced

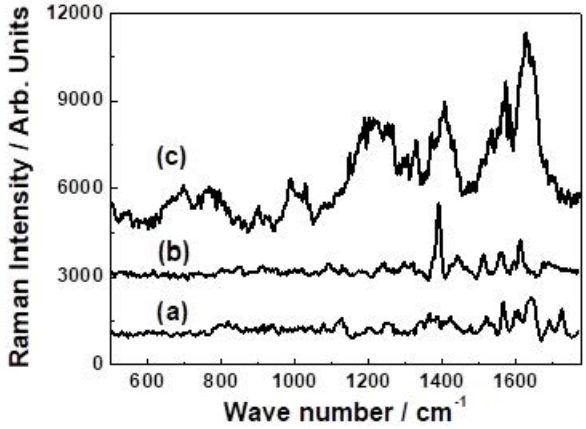

Figure 12. SERS spectrum of acetamiprid (Mospilan 20 SP) at concentrations of 2.25 mM **(a)**, 0.225 mM **(b)**, and 0.1125 mM **(c)** deposited on the annealed Ag covered 1 μm grade of manually polished (100) SiO_2 substrate.

from Figure 12 and Figure 13, where SERS spectra taken from covered 1 μm grade quartz substrate have about 2 times higher intensity with respect to these taken from Ag NSs 0.5 μm, respectively. This tendency is valid to the spectra taken from Ag NSs 0.1 μm with respect to the former one. This tendency was confirmed by the FDTD modeling.

The SERS spectra taken from three types of manually polished (100) SiO_2 substrates Au NP areas clearly have lower intensity compared with those taken from

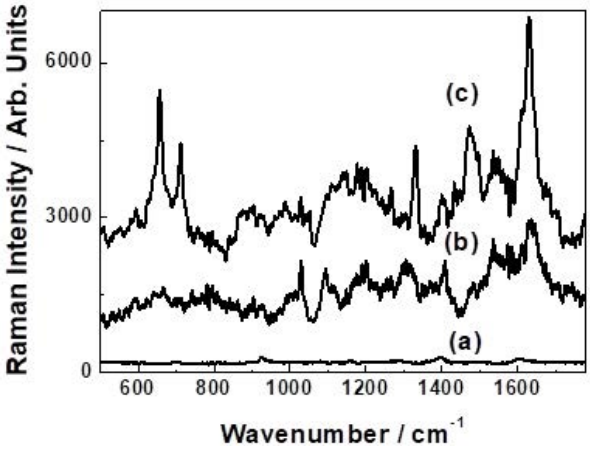

Figure 13. SERS spectrum of acetamiprid (Mospilan 20 SP) at concentrations of: 2.25 mM **(a)**, 0.225 mM **(b)**, and 0.1125 mM **(c)** deposited on the annealed Ag covered 0.5 μm grade of processed (100) SiO_2 substrate.

the corresponding Ag NPs. This is probably because of the lower plasmon resonance of Au NSs with respect to those of Ag NSs. It is worth noting that the bands presented by Chen [14] relayed for the pure acetamiprid powder. The bands at 624, 781, 1099, 1494, and 1588 cm^{-1} (Figure 12) coincided with these, achieved by Chen [14]. The band at 624 cm^{-1} can be ascribed to the N–C≡N wagging vibration. This is confirmed by to Han et al. [64] based on the theoretical calculations (density function theory-SERS). According to Phifer [15], the band at 1099 cm^{-1} was connected with CH in-plane deformation and CCC in-plane deformation vibrations (assigned by him as specific peak of acetamiprid), ring breathing vibration mode [65] or N–C stretching mode in the ring [64]. We can ascribe this band to the vibration of the ring of the acetamiprid molecule. Furthermore, the band at 1588 cm^{-1} can also be connected to the ring breathing vibration [64]. Another intensive band at 1416 cm^{-1} was reported by Hassan et al. [66].

The characteristic less intensive SERS peak at 364 cm^{-1}, which is observed from Ag NSs covering all grade polished (100) SiO_2 or in the Raman spectrum – 367 cm^{-1} can be associated with the vibration in the ring structure of the acetamiprid molecule [66]. Finally, two other intensive bands at 1612 and 1632 cm^{-1} were observed, which were not reported by other authors, which we can ascribe them to the distortion of the benzene-type ring. In fact, Han et al. [64] presented two bands in the range of 1600–1700 cm^{-1} obtained by density function theory – SERS calculated spectrum, unfortunately, with no discussions. The binding mechanism of Au or Ag NSs with acetamiprid molecule is probably missing or is very low. It is worth noting that chlorine atom in the acetamiprid molecule may be bonded to the Ag surfaces and thus may affect the SERS spectra or shift of some peaks. Additionally, in order to improve the acetamiprid SERS signal, Han et al. [64] removed the formation of silver oxide covering Ag nanorods by chemical ways. We did not apply any chemical treatments to the Ag films or Ag NPs.

The SERS results of Mospilan 20 SP (acetamiprid) were confirmed by FDTD modeling The FDTD modeling reveals higher enhancement effectiveness of the Ag NSs and being maximum for the Ag with 1 μm grade of quartz substrate and decreasing to two to three times for the Ag with 0.1 μm grade of quartz substrate. The SERS signal taken using Ag nanostructures was higher compared with those of Au NSs.

3.5 The enhancement factor (EF) and lowest detection limit (LOD)

Following the procedure described by Atanasov et al. [52], the enhancement factor (EF) based on the most effective and strongly expressed bands of Raman spectra of every neonic were evaluated. In brief, using well-known equation

$$\mathrm{EF} = I_{\mathrm{SERS}} N_{\mathrm{glass}} / I_{\mathrm{glass}} N_{\mathrm{SERS}} \,,$$

where I_{SERS} and I_{glass} are the peak intensity of the chosen strongest peaks in SERS and μ-Raman spectra, respectively, and N_{SERS} and N_{glass} are the numbers of neonic molecules in the area of the measured laser spot.

The highest value of EF about $\approx 10^5$ was achieved in the case of thiamethoxam [51, 52] deposited on PLD Ag and laser annealed films on (001) SiO_2 substrate or imidacloprid [56] deposited on Ag and Au and laser annealed films on 1-μm polished or back side Si wafer, respectively. It is worth noting that the goal of our works was not to show "a record value" but to demonstrate efficient substrates that are able to detect traces of the studied insecticide lower than applied in the agriculture.

A very advanced results were achieved when Ag NPs arrays were produced on the printing paper [53]. To the best of our knowledge, SERS spectra were obtained in the case of Aktara 25 BG deposited on Ag NPs arrays produced on paper substrate caused by plasmon resonance, thus, the enhanced factor of 10^4 was estimated.

For all investigated neonics, the lowest detection limit was estimated base on the values of the strongest SERS peaks. In case of acetamiprid it is presented in Figure 14. Here LOD was estimated to be about ~ 40 nM.

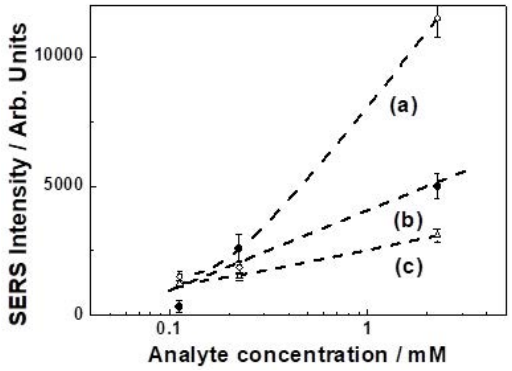

Figure 14. Surface-enhanced Raman spectra calibration curves of acetamiprid (Mospilan 20 SP) deposited on: **(a)** annealed Ag covered 1 μm grade manually polished (100) SiO_2 substrate, based on 1612 cm^{-1} band; **(b)** annealed Ag covered 0.5 μm grade manually polished (100) SiO_2 substrate, based on 1632 cm^{-1} band; and **(c)** ceramic/Ag substrate, based on 1416 cm^{-1} band. Calibration curve errors bars represent deviation of at least two identical measurements at maximum intensity.

In case of imidacloprid, LOD was evaluated to be about ~50 nM. Here Ag and Au NPs were deposited on Al_2O_3 ceramics. When pulsed-laser deposited and annealed Ag and Au films on 1-μm polished or back side Si wafer were produced, LOD is below <0.5 nM (Figure 15).

In case of thiacloprid, LOD is deduced to be about $\sim 2 \times 10^{-5}$ M as the EF increases up to $\approx 10^4$, when laser annealing was applied (Figure 16).

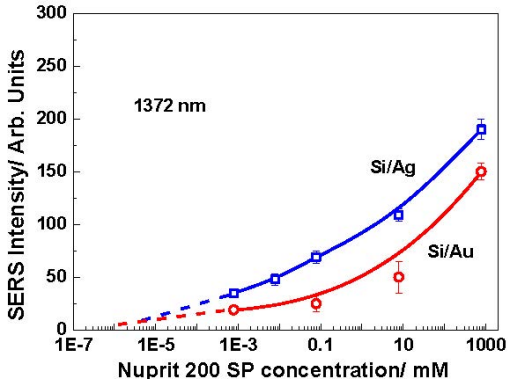

Figure 15. Surface-enhanced Raman spectra calibration curves of Nuprit 200 SP (imidacloprid) deposited on Au (red lines) or Ag (blue lines) NPs arrays produced on 1 μm processed Si substrate, based on the 1372 cm^{-1} band. The metal films were deposited by pulsed laser deposition and then annealed by 3 laser pulses. Calibration curves errors bars represent the deviation of the identical measurements at between three and sixes different points on the surfaces of the samples.

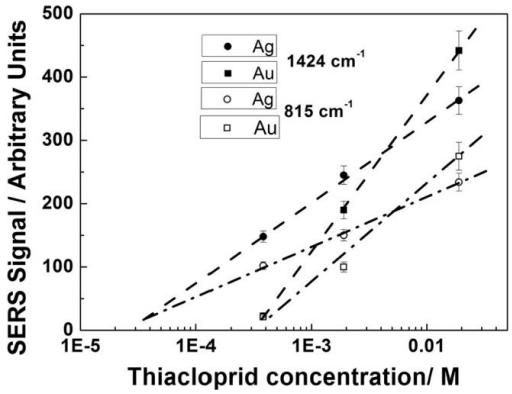

Figure 16. Surface-enhanced Raman spectra calibration curves of neonicotinoid insecticide Thiacloprid (Calypso 480 SC).

Finaly, the summary of the basic substrates used to create active Ag and Au nanostructures arrays for surface-enhanced Raman spectroscopy of neonicotinoids studied as well as the results of SERS achieved are presented in Table 2.

4 Conclusions

The investigations and results presented in this article can be summarized as follows: different new types advanced active Ag and Au nanostructured substrates

Table 2. Summary of the basic substrates used to create active Ag and Au nanostructures arrays for surface-enhanced Raman spectroscopy of studied neonicotinoids and the results of SERS

Basic substrate	**Method of deposition**	**Annealing**	LOD EF	**Neonics (studied)**	**Ref.**
1 μm micro-processed or back side Si wafer	thermal or pulsed laser deposition of Ag and Au films	pulsed laser	< 0.5 nM $\approx 8.8 \times 10^4$	imidacloprid (Nuprid 200 SP)	[50]
Al_2O_3 ceramic	thermal deposition of Ag and Au films		≈ 50 nM; 7.2×10^3	imidacloprid (Nuprid 200 SP, Warrant 700 WG)	[56]
(001) SiO_2	pulsed laser deposition of Ag films	pulsed laser	< 0.26 mM; $\approx 10^5$	thiamethoxam (Aktara 25 BG)	[51, 52]
Printer paper	pulsed laser deposition of Ag films	pulsed laser	≈ 1.28 mM; $\approx 10^4$	thiamethoxam (Aktara 25 BG)	[53]
Al_2O_3 ceramic	thermal deposition of Ag and Au films	pulsed laser	380 μM; $\approx 10^4$	thiacloprid (Calipso 480 SC)	[54]
1, 0.5 & 0.1 μm micro-processed (001) SiO_2	thermal deposition of Ag and Au films	pulsed laser	≈ 40 nM; 6.6×10^3	acetamiprid (Mospilan 20 SP)	[55]

were produced by pulsed-laser deposition or thermal deposition on several different basic substrates as Si wafers, quartz, paper, aluminum ceramics or diamond abrasive films in view of surface-enhanced Raman spectroscopy (SERS) detection of the 5 different neonicotinoids; in all cases the EF and LOD were evaluated.

Based on the results of the investigations presented several conclusions can be made:

- Si as basic substrate provides excellent opportunity with respect of surface morphology. Additionally, it is easy for making SEM analysis without covering the structure against charging during SEM measurements. The enhancement factor was estimated to be $> 5.10^4$ as the limit of detection reached was <0.5 nM – the best values regarding basic substrates used (see Table 2);
- The cheapest basic substrate was found to be the paper. However, it cannot be processed by thermal deposition because of its low burning temperature;

- Pulsed laser deposition is a better processing method compared to the thermal deposition for production of thin Ag or Au films since it provides excellent control of the thickness. On the contrary, thermal deposition is much easy to make but is very difficult to control exactly the thickness of the films;
- Further investigation of the neonics is becoming difficult since it is very complicated to find them on sale.

We hope that our study impact and contribute to the decision of EU Commission to banned the outdoor application of neonicotinoids in agriculture practice.

Acknowledgments

The Authors gratefully acknowledge the collaboration with Dr. Subramani, Prof. Terakawa and Dr. Y. Nakajima - Japan, Dr. Hirsch and Prof. Rauschenbach – Germany and Dr. Nikov and Prof. Dikovska – Bulgaria and the support of the National Institute for Materials Science (NIMS), Japan 2017-2022. The research that led to these results was carried out with the help of infrastructure purchased under the National Roadmap for Scientific Infrastructure (ELI-ERIC-BG), financially coordinated by the Ministry of Education and Science of the Republic Bulgaria under project D01-351.

References

[1] I. Yamamoto, J. Casida (1999) "*Nicotinoid Insecticides and the Nicotinic Acetylcholine Receptor*". Tokyo: Springer-Verlag.

[2] M. Tomizawa, J.E. Casida (2005) Neonicotinoid insecticide toxicology: mechanisms of selective action *Annu. Rev. Pharmacol. Toxicol.* **45** 247-268.

[3] FAO specifications and evaluations for agricultural pesticides (2014) Specification 637, 1-34.

[4] Official J. of the European Union (24.1.2019) L 22/1

[5] European Food Safety Authority (EFSA) (2016) *EFSA J.* **14**(6) 4610.

[6] Neonicotinoids: Risk to Bees Confirmed. In: *EFSA* (European Food Safety Authority) (2018) http://www.efsa.europa.eu/en/press/news/180228 (accepted Sep 4 2019).

[7] E. Watanabe (2012) Review on analytical methods with chromatographic and nonchromatographic techniques for new generation insecticide neonicotinoids. In: *Insecticides – advances in integrated pest managements* edited by F. Perveen. InteChOpen 22, pp. 481-510.

[8] A.A.G. Moreira, P. De Lima-Neto, E.W.S. Caetano, I.L. Barroso-Neto, V.N. Freire (2016) Computational electronic structure of the bee killer insecticide imidacloprid. *New J. Chem.* **40** 10353-10362.

[9] A.A.G. Moreira, P. De Lima-Neto, E.W.S. Caetano, I.L. Barroso-Neto, V.N. Freire (2017) The vibrational properties of the bee-killer imidacloprid insecticide: A molecular description. *Spectrochim. Acta - A: Mol. Biomol. Spectrosc.* **185** 245-255.

[10] S.R. Ahmed, K. Koh, E.Y. Park, J. Lee (2013) Toxic chemical monitoring of agricultural bioproducts using nanomaterials-based sensors. *Korean J. Chem. Eng.* **30** 1825-1832.

[11] H.-J. Kim, W.L. Shelver, E.-C. Hwang, T. Xu, Q.X. Li (2006) Automated flow fluorescent immunoassay for part per trillion detection of the neonicotinoid insecticide thiamethoxam. *Anal. Chim. Acta* **571**(1) 66-73.

[12] T. Xu, K.-Y. Wei, J. Wang, H.-X. Ma, J. Li, Y.-J. Xu, Q.X. Li (2010) Quantitative analysis of the neonicotinoid insecticides imidacloprid and thiamethoxam in fruit juices by enzyme-linked immunosorbent assays. *J. AOAC Int.* **93**(1) 12-18.

[13] F. Zhang, Y. Zhang, H. Ni, K. Ma, R. Li (2014) Experimental and DFT studies on the vibrational, electronic spectra and NBO analysis of thiamethoxam. *Spectrochim. Acta A Mol. Biomol. Spectrosc.* **118** 162-171.

[14] T. Chen (2014) Detection of Pesticide Residues on Apples Using Surface-Enhanced Raman Spectroscopy. Master of Science in Food Science Thesis. Minneapolis, MN, University of Minnesota.

[15] A.L. Phifer (2013) Analytical Techniques to Optimize Trace Insecticide Detection Mechanisms Using Surface Plasmon Resonance and Surface-Enhanced Raman Spectroscopy. Master of Science in Food Science Thesis. New York: Cornell University.

[16] M.V. Cañamares, A. Feis (2013) Surface-enhanced Raman spectra of the neonicotinoid pesticide thiacloprid. *J. Raman Spectrosc.* **44**(8) 1126-1135.

[17] N. Chamuah, N. Bhuyan, P.P. Das, N. Ojah, A.J. Choudhary, T. Medhi, P. Nath (2018) Gold-coated electrospun PVA nanofibers as SERS substrate for detection of pesticides. *Sens. Actuators B* **273** 710.

[18] T. Yaseen, H. Pu, D.-W. Sun (2019) Fabrication of silver-coated gold nanoparticles to simultaneously detect multi-class insecticide residues in peach with SERS technique. *Talanta* **196** 537-545.

[19] A. Laaniste, I. Leito, R. Rebane, R. Löhmus, A. Löhmus, F. Punga, A. Kruve (2016) Determination of neonicotinoids in Estonian honey by liquid chromatography–electrospray mass spectrometry. *J. Environ. Health, Part B* **51** 455-464.

[20] G. Quintás, S. Armenta, S. Garrigues, M. de la Guardia (2004) Fourier transform infrared determination of imidacloprid in pesticide formulations. *J. Braz. Chem. Soc.* **15** 307-312.

[21] S. Gerbig, H.E. Brunn, B. Spengler, S. Schulz (2015) Spatially resolved investigation of systemic and contact pesticides in plant material by desorption electrospray ionization mass spectrometry imaging (DESI-MSI). *Anal. Bioanal. Chem.* **407** 7379-7389.

[22] Y. Huang, J. Cao, S. Ye, J. Duan, L. Wu, Q. Li, S. Min, Y. Xiong (2013) Near-infrared spectral imaging for quantitative analysis of active component in counterfeit imidacloprid using PLS regression. *Optik* **124** 1644-1649.

[23] K.L. Lee, M.L. You, C.H. Tsai, E.H. Lin, S.Y. Hsieh, M.H. Ho, J.C. Hsu, P.K. Wei (2016) Nanoplasmonic biochips for rapid label-free detection of imidacloprid pesticides with a smartphone. *Biosens. Bioelectron.* **75** 88-95.

[24] A. Kruve, V. Bulatov, I. Schechter (2018) Quantitative and sensitive mapping of imidacloprid on plants using multiphoton electron extraction spectroscopy. *Chem. Phys.* **514** 126-131.

[25] H. Zhang, Y. Kang, P. Liu, X. Tao, J. Pei, H. Li, Y. Du (2016) Determination of pesticides by surface-enhanced Raman spectroscopy on gold-nanoparticle-modified polymethacrylate. *Anal. Lett.* **49** 2268-2278.

[26] A.M. Dowgiallo, D. Guenther (2017) Detection of Pesticide Residues on Fruit Surfaces Using Surface-Enhanced Raman Spectroscopy. *Ocean Optics* 1-8.

[27] R. Hou, S. Pang, L. He (2015) In situ SERS detection of multi-class insecticides on plant surfaces. *Anal. Methods* **7** 6325-6330.

[28] J. Tang, W. Chen, H. Ju (2019) Rapid detection of pesticide residues using silver nanoparticles coated glass bead as nonplanar substrate for SERS sensing. *Sens. Actuators B* **287** 576-583.

[29] Q. Chen, M.M. Hassan, J. Xu, M. Zareef, H. Li, Y. Xu, P. Wang, A.A. Agyekum, F.Y.H. Kutsanedzie, A. Viswadevarayalu (2019) Fast sensing of imidacloprid residue in tea using surface-enhanced Raman scattering by comparative multivariate calibration. *Spectrochim. Acta - A: Mol. Biomol. Spectrosc.* **211** 86-93.

[30] C. Noguez (2007) Surface plasmons on metal nanoparticles: the influence of shape and physical environment. *J. Phys. Chem. C* **111** 3806-3819.

[31] A. Plech, P. Leiderer, J. Boneberg (2009) Femtosecond laser near field ablation. *Laser & Photon. Rev.* **3** 435-451.

[32] M.I. Stockman (2011) Nanoplasmonics: past, present, and glimpse into future. *Opt. Express* **19** 22029-22106.

[33] M. Moskovits (2005) Surface-enhanced Raman spectroscopy: a brief retrospective. *J. Raman Spectrosc.* **36**(6,7) 485-496.

[34] N. Nedyalkov, T. Sakai, T. Miyanishi, M. Obara (2006) Near field properties in the vicinity of gold nanoparticles placed on various substrates for precise nanostructuring. *J. Phys. D: Appl. Phys.* **39** 5037.

[35] S. Kawata (2001) In: "*Near-Field Optics and Surface Plasmon Polaritons*" edited by S. Kawata, M. Ohtsu, M. Irie, Vol. 81. Springer Science & Business Media, Berlin.

[36] G.A. Baker, D.S. Moore (2005) Progress in plasmonic engineering of surface-enhanced Raman-scattering substrates toward ultra-trace analysis. *Anal. Bioanal. Chem.* **382**(8) 1751-1770.

[37] M.K. Fan, G.F.S. Andrade, A.G. Brolo (2011) A review on the fabrication of substrates for surface enhanced Raman spectroscopy and their applications in analytical chemistry. *Anal. Chim. Acta* **693** 7-25.

[38] K. Kneipp, Y. Wang, H. Kneipp, L.T.; Perelman, I. Itzkan, R.R. Dasari, M.S. Feld (1997) Single molecule detection using surface-enhanced Raman scattering (SERS). *Phys. Rev. Lett.* **78**(9) 1667.

[39] B. Sharma, R.R. Frontiera, A.I. Henry, E. Ringe, R.P. Van Duyne (2012) SERS: Materials, applications, and the future. *Materials Today* **15**(1-2) 16-25.

[40] C.L. Haynes, A.D. McFarland, R.P. Van Duyne (2005) Surface-enhanced Raman spectroscopy. *ACS Publications, Anal. Chem.* **77** 338A-346A.

[41] P.L. Stiles, J.A.; Dieringer, N.C. Shah, R.P. Van Duyne (2008) Surface-enhanced Raman spectroscopy. *Annu. Rev. Phys. Chem.* **1** 601-626.

[42] K.A. Willets, R.P. Van Duyne (2007) Localized surface plasmon resonance spectroscopy and sensing. *Annu. Rev. Phys. Chem.* **58** 267-297.

[43] R.G. Freeman, K.C. Grabar, K.J. Allison, R.M. Bright, J.A. Davis, A.P. Guthrie, M.B. Hommer, M.A. Jackson, P.C. Smith, D.G. Walter, M.J. Natan (1995) Self-assembled metal colloid monolayers: an approach to SERS substrates. *Science* **267**(5204) 1629-1632.

[44] M.J. Banholzer, J.E. Millstone, L.D. Qin, C.A. Mirkin (2008) Rationally designed nanostructures for surface-enhanced Raman spectroscopy. *Chem. Soc. Rev.* **37**(5) 885-897.

[45] R.L. McGreery (2000) "*Raman spectroscopy for chemical analysis*". John Wiley & Sons Inc, NY.

[46] W.E. Smith, P.C. White, C. Rodger, G. Dent (2001) "*Handbook of Raman Spectroscopy*" edited by I.R. Lewis and H.G.M. Edwards. Marcel Dekker, Inc. New York, pp. 733-48.

[47] T. Vo-Dihn, D.L. Stokes (2002) "*Handbook of Vibrational Spectroscopy*" 2, edited byJ.M. Chalmers and P.R. Griffiths. John Wiley & Sons Ltd, Chichester, pp. 1302-1317.

[48] J.M. Chalmers, H.M. Edwards, M.D. Hargreaves (2012) "*Infrared and Raman Spectroscopy in Forensic Science*". John Wiley & Sons, ch. 45-86.

[49] W.W. Yu, I.M. White (2013) Inkjet-printed paper-based SERS dipsticks and swabs for trace chemical detection. *Analyst* **138**(4) 1020-1025.

[50] P.A. Atanasov, N.N. Nedyalkov, A.O. Dikovska, N. Fukata, W. Jevasuwan (2023) SERS active substrates for neonicotinoids studies. *J. Phys.: Conf. Ser.* **2487** 012012.

[51] P.A. Atanasov, N.N. Nedyalkov, Ru. Nikov, N. Fukata, W. Jevasuwan, T. Subramani, D. Hirsch, B. Rauschenbach (2017) SERS of Insecticides and Fungicides assisted by Au and Ag nanostructures produced by laser techniques. *Int. J. Environ. Agric. Res.* 3(4) 61-69.

[52] P.A. Atanasov, N.N. Nedyalkov, Ru. Nikov, N. Fukata, W. Jevasuwan, T. Subramani, D. Hirsch, B. Rauschenbach (2018) SERS analyses of thiamethoxam assisted by Ag films and nanostructures produced by laser techniques. *J. Raman Spectrosc.* **49**(3) 397-403.

[53] P.A. Atanasov, N.N. Nedyalkov, N. Fukata, W. Jevasuwan, T. Subramani, M. Terakawa, Y. Nakajima (2019) Surface-enhanced Raman spectroscopy (SERS) of mancozeb and thiamethoxam assisted by gold and silver nanostructures produced by laser techniques on paper. *Appl. Spectrosc.* **73**(3) 313-319.

[54] P.A. Atanasov, N.N. Nedyalkov, N. Fukata, W. Jevasuwan, T. Subramani (2020) Surface-enhanced Raman spectroscopy (SERS) of neonicotinoid insecticide thiacloprid assisted by silver and gold nanostructures. *Appl. Spectrosc.* **74**(3) 357-364.

[55] P.A. Atanasov, N.N. Nedyalkov, N. Fukata, W. Jevasuwan (2020) Ag and Au nanostructures for surface-enhanced Raman spectroscopy of Mospilan 20 SP (acetamiprid). *J. Raman Spectrosc.* **51**(12) 2398-2407.

[56] P.A. Atanasov, N.N. Nedyalkov, N. Fukata, W. Jevasuwan, T. Subramani (2020) Surface-enhanced Raman spectroscopy of neonicotinoid insecticide imidacloprid, assisted by gold and silver nanostructures. *Spectrosc. Lett.* **53**(3) 184-193.

[57] A. Taflove, S.C. Hagness (2000) "*Computational Electrodynamics: The Finite-Difference Time-Domain Method*". Artech House, Boston, MA.

[58] D. Sullivan, J. Liu, M. Kuzyk (2000) Three-dimensional optical pulse simulation using the FDTD method. *IEEE Trans. Microw. Theory Tech.* **48**(7) 1127-1133.

[59] N.N. Nedyalkov, P.A. Atanasov, M. Obara (2007) Near-field properties of a gold nanoparticle array on different substrates excited by a femtosecond laser. *Nanotechnology* **18** 305703.

[60] P.B. Johnson, R.W. Christy (1972) Optical constants of the noble metals. *Phys. Rev. B.* **6** 4370.

[61] E.D. Palik (1998) "*Handbook of Optical Constants of Solids*" Vol. 3. Academic Press.

[62] M.L. Nicholas, D.L. Powel, T.R. Williams, R.H. Bromund (1976) Reference Raman spectra of DDT and five structurally related pesticides and of five pesticides containing the norbornen group. *J. AOC* **59**(1) 197-208.

[63] W.C. Zhang, X.L. Wu, C.X. Kan, F.M. Pan, H.T. Chen, J. Zhu, P.K. Chu (2010) Surface-enhanced Raman scattering from silver nanostructures with different morphologies. *Appl. Phys. A: Mater. Sci. Process*. **100** 83-88.

[64] C.-Q. Han, Y. Yao, W. Wang, L.-Q. Tao, W.-X. Zhang, W.M. Ingram, K.-Z. Tian, Y. Liu, A.-X. Lu, Y. Wu, C.-C. Yan, L.-L. Qu, H.-T. Li (2018) Highly sensitive silver nanorod arrays for rapid surface enhanced Raman scattering detection of acetamiprid pesticides. *Chin. J. Chem. Phys*. **31**(2) 152-158.

[65] W. Wijaya, S. Pang, T.P. Labuza, L. He (2014) Rapid detection of acetamiprid in foods using Surface-Enhanced Raman Spectroscopy (SERS). *J. Food Sci*. **79**(4) T743-T747.

[66] M.M. Hassan, Q. Chen, F.Y. Kutsanedzie, H. Li, M. Zareef, Y. Xu, M. Yang, A.A. Agyekum (2019) rGO-NS SERS-based coupled chemometric prediction of acetamiprid residue in green tea. *J. Food Drug Anal*. **27**(1) 145-153.